8670 *Macromolecules* **2010**, *43*, 8670–8685
DOI: 10.1021/ma101421s

Macromolecules
ARTICLE

Rheology and Morphology of Dynamically Asymmetric LCST Blends: Polystyrene/Poly(vinyl methyl ether)

Jafar Khademzadeh Yeganeh, Fatemeh Goharpey,* and Reza Foudazi

Department of Polymer Engineering, Amirkabir University of Technology, Tehran, Iran

Received June 27, 2010; Revised Manuscript Received September 13, 2010

ABSTRACT: We investigated the correlation between the time evolution of the different phase-separating morphologies and corresponding linear and transient rheological behaviors for the dynamically asymmetric PS/PVME blend in which there is a large difference between glass transitions of the pure components (about 125 °C). The phase diagram was obtained from dynamic temperature sweep experiments. Phase contrast optical microscopy was employed to investigate morphological evolution of PS/PVME blends at various regions of obtained phase diagram at a constant temperature of 105 °C. At this temperature depending on sample composition, the viscoelastic phase separation (VPS) was observed besides the usual phase separation mechanisms (nucleation and growth (NG) and spinodal decomposition (SD)), indicating the interplay between thermodynamics and viscoelasticity in phase-separation behavior of PS/PVME blends. The linear viscoelastic behavior for different phase separating mechanisms (NG, SD, and VPS) was measured to investigate the kinetics of phase separation. It was found that the linear viscoelastic behavior can be described by Palierne's emulsion model, if the self-generated stresses induced during the phase separation in the matrix phase are taken into account. Furthermore, the stress growth behavior of different phase-separating morphologies was investigated by transient start-up of shear flow.

1. Introduction

Phase separation behavior of polymer blends has attracted great interest from both scientific and industrial viewpoints,[1−15] since some issues such as effect of viscoelasticity on phase separation,[1−5] phase separation mechanism in metastable region,[6,7] phase separation under shear flow,[8,9] and kinetics of phase separation[10,11] are not well understood yet. In the recent years, rheology as a sensitive tool to morphological changes has been widely used to study phase behavior of polymer blends in the two-phase region and in the vicinity of the phase separation[15−22] that involves complex combinations of kinetics, thermodynamics, and viscoelasticity.

In the vicinity of phase separation, where the mass fluctuation is accomplished through the reptation of molecular chains, the fluctuations induce extra shear stress and hence elevate the storage modulus G' and the loss modulus G'' to larger extents.[12] Ajji et al.[13] used the theoretical treatment of Fredrickson and Larson[14] to explain this phenomenon. Fredrickson and Larson employed the mean-field theory to derive the concentration fluctuation contribution to the shear stress for near-critical polymer mixtures. Experimentally, Kapnistos,[15] Sharma,[16] and Gharachorlou et al.[17] extended this analysis for the off-critical components to obtain spinodal temperatures. They[15−17] attributed the enhancement of elasticity near the phase separation to concentration fluctuations and believed that there also exists a fluctuation dominant region in metastable region. However, Bousmina[18] and Niu et al.[11] argued that this theory fails to predict spinodal temperatures correctly, and the origin of enhancement of elasticity near phase separation is due to the emergence of interface.

In polymer blends, upon variation in temperature, pressure, and/or composition, phase separation can occur by nucleation and growth (NG) or spinodal decomposition (SD) mechanisms. In the past decade, Tanaka found a new type of phase separation in dynamically asymmetric mixtures, which is called viscoelastic phase separation (VPS).[1−5] Dynamic asymmetry in polymer blends can be induced by a large difference in glass transition temperature between the components of a mixture. The main feature of VPS is the induction of a percolating network of the more viscoelastic phase even if volumetrically is the minor phase which is in contrast to the normal phase separation (NPS), where the minor phase is in the form of isolated droplets. This percolated network structure coarsens in time and eventually breaks into disconnected domains; in other words, phase inversion occurs. The phase separation of PS and PVME mixture is one of the most well-studied polymer blends which has been believed for a long time to behave as a normal phase separation system.[23,24] However, Tanaka observed that for the PS/PVME blend at quench depth of about 20 °C above LCST phase separation took place by the VPS mechanism.[4] Tanaka argued that due to the large difference in glass-transition temperature between PS and PVME (about 130 °C), deep quench leads to a large difference in the viscoelastic properties of coexisting phases; hence, VPS will control phase behavior. However, in our previous work[17] and in other investigations,[23,24] even for much deeper quenches, VPS has not been observed and NPS controlled phase behavior. This indicates that in dynamically asymmetric polymer blends further investigations should be done to understand that under what conditions phase separation takes place through the VPS or NPS mechanism.

Studying the correlation between the resulted phase-separated morphologies and their rheological behavior has been the subject of different studies, both experimentally and theoretically.[19−22] The linear viscoelastic behavior of polymer blends with a droplet-matrix morphology can be described quantitatively[25] by the Palierne's emulsion model.[26] Moreover, this model has been widely used to obtain either the interfacial tension or structural information (domain size and distribution) from dynamic

*Corresponding author: Tel +98 21 64542437, Fax +98 21 44210498, e-mail goharpey@aut.ac.ir.

 Published on Web 09/28/2010

measurements.[19,27] However, there are not enough studies of the Palierne's emulsion model for the phase-separating morphologies, especially for dynamically asymmetric blends.

Different observations have been made for time evolutions of the dynamic moduli in either the metastable or unstable regions. Vinckier et al.[21] observed that the storage modulus, G', monotonically decreased with time during phase separation in the unstable region due to the reduced interfacial area. A similar result was observed by Niu et al.[10,11] and Polios et al.[20] in the unstable region. However, Kim et al.[22] observed that in the unstable region there was a slight increase of storage modulus, and after passing through a maximum, G' decreased and reached equilibrium at the late stages. In the metastable region, Vinckier et al.[21] observed that G' monotonically increased with phase separation time, which was attributed to the deformability of larger droplets. However, in the metastable region, Niu et al.[10,11] observed that G' monotonically decreased with phase separation time.

Recently, the start-up of shear flow experiment has become the subject of experimental and theoretical investigations for polymer blends.[28−33] The transient character of this flow regime is an open complex problem that involves a complex relationship between flow and structure. In spite of the various results reported in the literature regarding the stress growth in the start-up experiment, many issues such as effect of domain size, elasticity of the components, and different morphologies on the rheological behavior are not fully understood, and to date, reported researches in the area of phase-separating polymer blends in the transient regime are rather scarce.

In this work, PS/PVME blends which exhibit a lower critical solution temperature (LCST) within the experimental temperature window were chosen for morphological and rheological studies. There are many studies on PS/PVME blends such as the kinetics of phase separation,[34] phase separation morphology,[23,24] segmental mobility,[35] the effect of molecular weight on the phase behavior,[36] and shear-induced mixing (SIM) and demixing (SID).[8,9] In addition, as mentioned above due to the large difference in glass-transition temperature between PS and PVME (about 130 °C), VPS can be induced in PS/PVME blends.[4]

The main objective of this work was theoretical and experimental investigations of the correlation between the evolution of different phase-separating morphologies and corresponding linear rheological behavior as well as stress growth response upon start-up of shear flow for PS/PVME blends. The effect of viscoelasticity on the phase separation behavior was examined as well. To the best of our knowledge, there is no study on the rheological behavior of phase-separating blends under VPS mechanism and its comparison with SD and NG ones in the literature. For this purpose, the phase diagram of PS/PVME blend was obtained, and then different compositions were chosen at various regions of obtained phase diagram to have different induced morphologies for rheological investigations.

2. Theoretical Background

The quantitative study of phase separation can be performed using the theoretical approach of Ajii and Choplin[13] for homopolymer blends. This approach is an extension of Fredrickson and Larson's theory[14] for block copolymer melts near the order−disorder transition.

Ajji and Choplin[13] found the following expressions for G' and G'' in terminal one-phase region in the vicinity of critical point:[12,17]

$$G'(\omega) = \frac{k_B T \omega^2}{240\pi}\left[\frac{1}{3}\left\{\frac{R_{g1}{}^2}{\phi_1 N_1}+\frac{R_{g2}{}^2}{\phi_2 N_2}\right\}\right]^{1/2}\left[\frac{1}{\phi_1 b_1{}^2 W_1}+\frac{1}{\phi_2 b_2{}^2 W_2}\right]^2 [2(\chi_s-\chi)]^{-5/2} \quad (1)$$

$$G''(\omega) = \frac{k_B T \omega}{240\pi}\left[\frac{1}{3}\left\{\frac{R_{g1}{}^2}{\phi_1 N_1}+\frac{R_{g2}{}^2}{\phi_2 N_2}\right\}\right]^{1/2}\left[\frac{1}{\phi_1 b_1{}^2 W_1}+\frac{1}{\phi_2 b_2{}^2 W_2}\right]^2 [2(\chi_s-\chi)]^{-1/2} \quad (2)$$

In the above equations, χ_s stands for the interaction parameter at the spinodal temperature, χ is the interaction parameter at temperature T, ϕ_i is the volume fraction of species i, N_i is the number of statistical segments, b_i is the statistical segment length, W_i is the rate of its reorientation, ω is the angular frequency, k_B is the Boltzmann coefficient, and R_{gi} is the radius of gyration. Using the above equations, the following ratio can be defined:

$$\frac{G'(\omega)}{[G''(\omega)]^2} = \frac{30\pi}{k_B T}\left\{\frac{b_1{}^2}{36\phi_1}+\frac{b_2{}^2}{36\phi_2}\right\}^{3/2}(\chi_s-\chi)^{-3/2} \quad (3)$$

It should be noticed that in this equation both the monomeric friction coefficient and the frequency dependence were eliminated. Assuming that the interaction parameter is given by

$$\chi = A+\frac{B}{T} \quad (4)$$

by substituting the interaction parameter in eq 3, one can find the following expression:

$$\left(\frac{G''2}{TG'}\right)^{2/3} = \frac{B}{C}\left(\frac{1}{T_s}-\frac{1}{T}\right) \quad (5)$$

where C is given by

$$C = \left(\frac{45\pi}{k_B}\right)^{2/3}\left[\frac{b_1{}^2}{\phi_1}+\frac{b_2{}^2}{\phi_2}\right] \quad (6)$$

Thus, there would be a linear dependence of $((G'')^2/(G'T))^{2/3}$ vs $1/T$, at the phase transitional region, in which the intercept with the $1/T$ axis is denoted as the reciprocal of the spinodal decomposition temperature, T_s.

3. Experimental Section

3.1. Materials. A commercial grade of PS (polystyrene) supplied by Tabriz Petrochemical Co. (GPPS grade 1160), PVME (poly(vinyl methyl ether)), and Lutonal M40, supplied by BASF Co., were used in this study. The basic characteristics of the polymers are listed in Table 1. Considering the chemical sensitivity of PVME, utmost cares were taken to prevent its oxidation. This can also be ensured by a simple visual observation of the blend; the sample should look transparent with a slight yellowish color.[37] Thermal gravimetric analysis (TGA) was also performed on PVME using Perkin-Elmer Pyris1 TGA system to be sure about its thermal stability during morphological and rheological analysis. It was found that the employed PVME is stable up to 192 °C in temperature sweep mode with 10 °C/min ramp and more than 4 h in time sweep mode at 105 °C.

3.2. Sample Preparation. The PS/PVME blends were prepared by continuous mechanical mixing of the components in toluene. The solvent was evaporated slowly at room temperature for

Table 1. Characterization of PS and PVME Used in This Study

	M_w (g/mol)	M_n (g/mol)	T_g (°C)	supplier
PS	248 000	87 000	93.5	Tabriz Petrochemical Co.
PVME	110 000	64 000	−32	BASF

1 week. Then the samples were put in a vacuum oven for 4 days at 45 °C. The vacuum was applied slowly to prevent any possible bubble formation. Finally, the full vacuum was applied at 70 °C for 24 h in order to remove the residual solvent remaining in the samples.[15,17] Weighting the samples and checking the value to match asymptotically with the total weight of the components ensured us the complete evaporation of solvent.

3.3. Methods. *Rheological Measurements*. All the rheological measurements were performed by a stress/strain-controlled rheometer (UDS 200, Paar Physica). The experiments were carried out using parallel plates geometry with 25 mm diameter and 1 mm gap. All the experiments were carried out under a continuous flow of nitrogen gas around the sample pan, and a fresh sample was used for each measurement.

The following small-amplitude oscillatory shear experiments were carried out in the linear viscoelastic region, as was verified by preliminary amplitude sweep tests: (i) Isochronal dynamic temperature sweep was carried out by measuring storage and loss moduli at a fixed frequency of 0.05 Hz, which was found to be low enough to lie in the terminal region in agreement with literature data,[15,16] and a uniform rate of heating (0.5 °C/min) from the homogeneous to the phase-separated regime at a certain strain (1%) in order to detect the onset of the phase separation. (ii) Dynamic time sweep experiments were performed in the phase-separated region at a fixed frequency of 1 rad/s and a given strain of 5% in order to investigate phase separation kinetics. According to Kim et al.,[22] rheological measurements with these conditions can sensitively detect the early stage of phase separation. (iii) Isothermal dynamic frequency sweep experiments were carried out at strain of 1% and temperature of 105 °C in order to study the linear viscoelastic properties. For samples at the two-phase region, measurements were performed after various preheat times at 105 °C to have desired phase-separated morphologies.

To study stress growth behavior of PS/PVME blends, start-up of simple shear flow were applied on samples at shear rate of $0.2\ s^{-1}$ and temperature of 105 °C. For samples at the two-phase region, measurements were carried out after various preheat times at 105 °C to have desired phase-separated morphologies.

Optical Microscopy (*OM*). Samples for optical microscopy were also prepared as mentioned in section 3.2. However, the thickness of samples for OM was approximately 25−30 μm. This is considerably thicker than the critical thickness (5−8 μm thin films) found by Reich and Cohen,[38] above which there is no dependence of the phase behavior on the film thickness and substrate. The phase contrast optical microscopy (Leica DMRX) was used to investigate morphological changes at constant temperature of 105 °C. Samples were placed in a hot stage sample holder (Linkam LTS350) which was controlled by the hot stage controller (Linkam CI 94). Fresh nitrogen gas was circulated in the heating chamber of OM to avoid any possible thermal degradation. A CCD camera mounted directly on the microscope allowed the recording of the evolution of blends structure in real time.

4. Results and Discussion

4.1. Determination of Phase Diagram. To obtain the phase diagram of PS/PVME blends, isochronal dynamic temperature sweep tests were carried out for various compositions as described in the Experimental Section. A typical curve of elastic modulus (G') and loss modulus (G'') vs temperature for 40/60 PS/PVME blend sample is shown in Figure 1.

It can be seen that at low temperatures the elastic modulus decreased with temperature rise. This is attributed to the greater mobility of the polymer chains or decreasing of intermolecular friction as sample moves away from its glass transition temperature. In the vicinity of phase separation temperature, there is always a competition between mobility and thermodynamics. As the temperature approached the phase segregation temperature, the thermodynamic forces

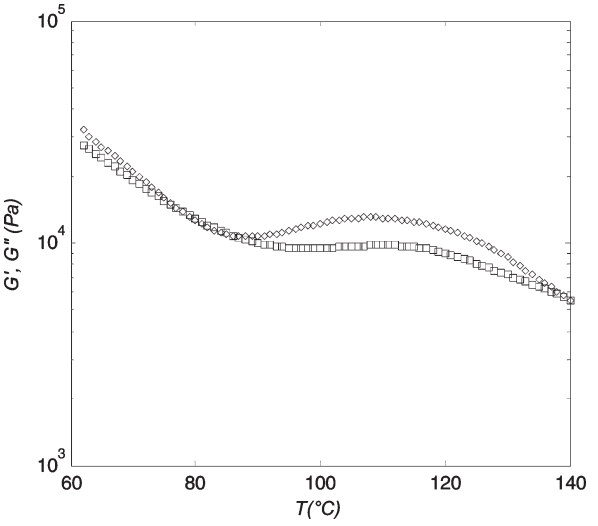

Figure 1. Temperature dependence of storage modulus, G' (◇), and loss modulus, G'' (□), for the PS/PVME 40/60 blend with frequency of $f = 0.05$ HZ, strain of 1%, and a heating rate of 0.5 °C.

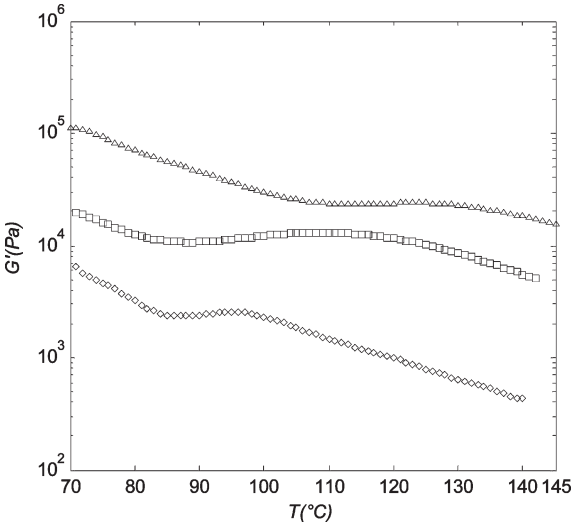

Figure 2. Temperature dependence of storage modulus of PS/PVME blends with the composition of 30/70 (◇), 40/60 (□), and 60/40 (△). Measured at frequency of $f = 0.05$ Hz and strain of 1%.

became dominant and increased the magnitude of G' (upturn in G' curve) by formation of dynamic domains, rich in the hard PS component of the blend.[15,17] Moreover, during the phase separation, the interface comes into play by introducing a supplementary elasticity in the system due to the deformation and the shape recovery of the formed domains.[18] By further increase in temperature, mobility forces controlled again the viscoelastic behavior of the phase separating blend, and G' decreased again. The temperature at the inflection point of G' vs temperature curve (between the maximum and minimum in the G' vs temperature curve) was found empirically corresponding to the binodal temperature of the blend sample.[7,11,15] The variation of G'' also exhibited similar behavior; however, it had less sensitivity with a phase lag which is in agreement with observed behavior of diblock copolymers[39] and supported by the prediction of mean-field theory as well.[13,14] The higher sensitivity of G' is attributed to the elastic origin of the stress induced to the system by concentration fluctuations. In mechanical analogy (Maxwell model), the elastic component responds faster and more significantly to a given deformation, as compared to the viscous component.

Figure 2 depicts the G' vs temperature behavior of PS/PVME blends for different compositions. It is evident that both the magnitude of G' upturn and the temperature range over which this upturn took place strongly depend on the composition of the blend. For the 30/70 blend (as will be shown that it was the critical composition), the magnitude of G' upturn was more obvious, and the corresponding transitional zone was also narrower than that of other compositions, which was thought to be due to different phase separation mechanism with larger concentration fluctuations and faster kinetics of phase separation (spinodal concentration fluctuations).

To obtain the spinodal temperatures of our studied blend samples, we applied Ajji and Choplin's[13] approach of Fredrickson−Larson theory (see the section 2). Figure 3 shows a typical plot of $((G'')^2/(G'T))^{2/3}$ against reciprocal temperature for the 30/70 blend. The slop of the curve in the linear region, which is corresponding to the one-phase region near the critical point, was taken and the inverse of the intercept with the $1/T$ axis was assumed to be the spinodal temperature, T_s. In this study, the determination of T_s involves an error of about ±2 °C.

To obtain the spinodal and binodal temperatures, we also applied Flory−Huggins theory. The interaction parameter was obtained by fitting the rheologically determined binodal temperatures with Flory−Huggins theory as a function of blend composition (ϕ) and temperature (T), as suggested by Kim et al.:[40]

$$\chi = 8.658e-5+\frac{-0.0285+0.01709\phi_{\mathrm{PVME}}}{T}\frac{\mathrm{mol}}{\mathrm{cm}} \quad (7)$$

The binodal and spinodal curves calculated from the Flory−Huggins theory by using eq 7 is shown in Figure 4. In the calculation of binodal and spinodal curves, the specific volumes of PS, ν_{PS}, and PVME, ν_{PVME}, were calculated as follows:[41,42]

$$\nu_{\mathrm{PS}} = 0.9199+5.098\times10^{-4}(T-273)+2.354\times10^{-7}(T-273)^2+[32.46+0.1017(T-273)]/M_{\mathrm{w,PS}} \quad (8)$$

$$\nu_{\mathrm{PVME}} = 1/[1.0717-7.67\times10^{-4}(T-273)+2.8\times10^{-7}(T-273)^2] \quad (9)$$

where $M_{w,PS}$ is the molecular weight of PS. Figure 4 shows the obtained phase diagram of PS/PVME blends which exhibited a lower critical solution temperature (LCST) with critical point located at temperature of about 94 °C and composition of PS/PVME 30/70.

It should be noted that due to the small strain and very low shear rate exerted on the sample in the small-amplitude oscillatory flow, it can be assumed that flow does not interfere with thermodynamics and kinetics of the phase separation for most polymer blend systems,[8,10,11,16−23,43] particularly in the case of PS/PVME blend samples.[8,16,17,20,22,43] However, Zhang et al.[12] showed that oscillatory flow can induce shear demixing for the polybutadiene (PB)/low vinyl content polyisoprene (LPI) polymer blend system.

Increasing heating rate[15] or frequency[12] of rhological measurements could lead to higher measured phase separation temperatures; however, according to the literature, low heating rates (below 1 °C/min) and low frequencies give reliable phase diagram compared to that obtained by static methods, such as laser light transmission,[43] DSC,[17,43] turbidity

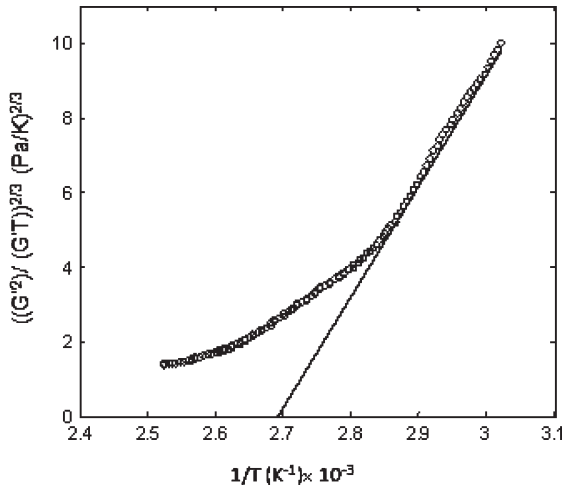

Figure 3. Quantitative evaluation of the viscoelastic behavior of 30/70 blend near the phase separation and determination of the spinodal temperature.

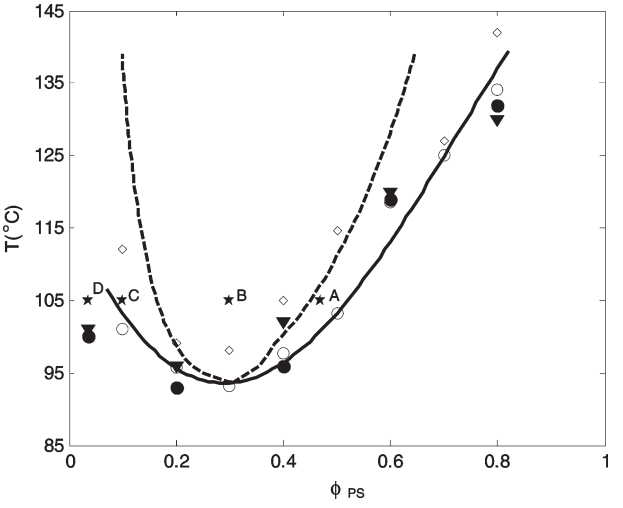

Figure 4. Phase diagram of PS/PVME blends determined from (i) rheological measurement: binodal temperature (○) spinodal temperature (◇); (ii) Flory−Huggins theory: binodal curve (—); spinodal curve (---); (iii) binodal temperature from DSC (▼) and turbidity measurements (●). Selected PS/PVME blends for morphological and rheological investigations are shown with the (★) symbol with the weight compositions of (A) 46/54, (B) 30/70, (C) 10/90, and (D) 3.5/96.5.

temperature measurements,[8,17,43] and optical micrographs of morphology development.[10] The difference between phase separation temperatures obtained by different procedures for PS/PVME blend samples is about 5 °C. To verify the obtained phase diagram in this work, the DSC results and turbidity measurements from our previous work for the same blend samples[17] are shown in the Figure 4 as well. The morphological analysis performed during the phase separation at various regions of phase diagram (section 4.2) also supported the rheologically determined phase diagram, except for very low concentrations of PS where thermal and optical methods showed better prediction which could be due to less sensitivity of bulk rheology for such very dilute blend samples. However, the objective of this work is not to compare the phase diagram obtained by different thermal, morphological, and rheological methods.

It can be seen that the spinodal temperatures determined by rheological data (Fredrickson−Larson theory) were slightly scattered. Moreover, the rheologically determined

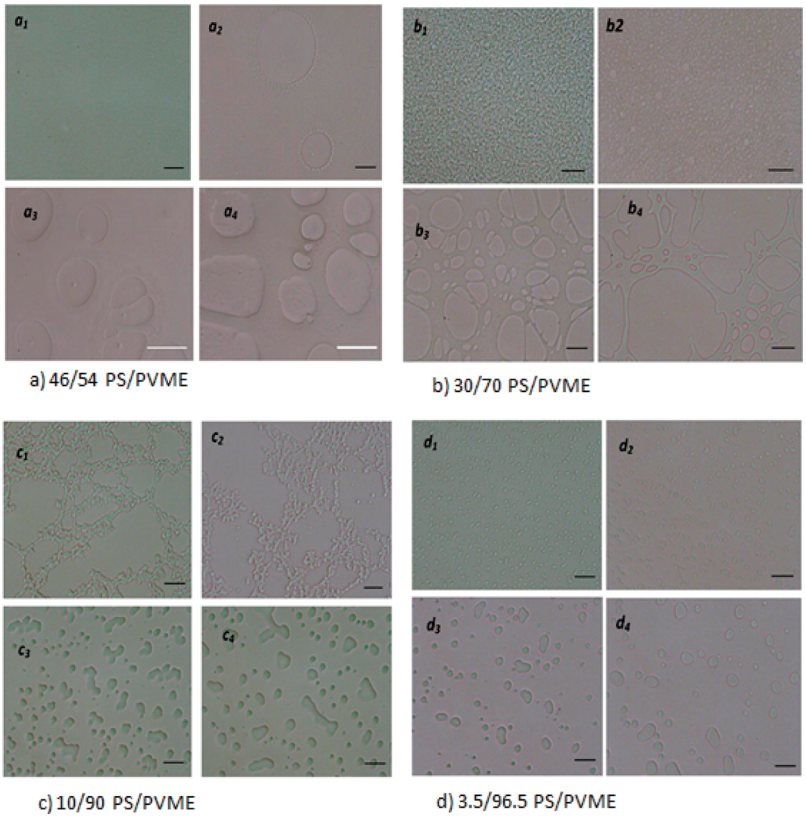

Figure 5. Optical micrographs indicating time evolution of the phase-separating morphologies for PS/PVME blends with the compositions: (a) 46/54 annealed at 105 °C for (a_1) 30 min, (a_2) 4 h, (a_3) 5 h, (a_4) and 7 h; (b) 30/70 annealed at 105 °C for (b_1) 20 min, (b_2) 50 min, (b_3) 2 h, and (b_4) 3 h; (c) 10/90 annealed at 105 °C for (c_1) 2 h, (c_2) 3 h, (c_3) 4 h, and (c_4) 5 h; (d) 3.5/96.5 annealed at 105 °C for (d_1) 30 min, (d_2) 2 h, (d_3) 3 h, and (d_4) 4 h. All the black scale bars correspond to 10 μm, and the white ones correspond to 50 μm.

spinodal temperature in the critical composition was not superimposed on the minimum binodal temperature, with a gap of about 6 °C. Similar observations have been reported by Bousmina et al.[18] and Niu et al.[11] This behavior can be attributed to the simplifying assumptions used by Ajji and Choplin to develop the approach and also to the error encounters by the selection of the linear range in determining the spinodal temperatures. The following simplifying assumptions can be inferred in their approach: (i) the absence of the interaction parameter in the Onsager coefficient equation;[18] (ii) the constant friction coefficient for species 1 in the mixture of 1 and 2;[18] (iii) neglecting the intermolecular entanglement of polymer chains; (iv) neglecting the concentration dependence of interaction parameter (see eq 4).

In spite of the above discussion, the spinodal line determined by the rheological measurements reasonably agreed with that obtained from Flory−Huggins theory and can provide us simply the boundary of unstable region and/or useful experimental evidence for the further investigations on the phase separation kinetics of the blends, as was shown in our previous work.[17]

4.2. Morphological Observations. In order to support the obtained phase diagram and to have a deep insight into the morphology development, we carried out optical microscopy observation during the phase separation for PS/PVME blends at various regions of the phase diagram for weight compositions of 46/54, 30/70, 10/90, 5/95, and 3.5/96.5 (★ symbols in Figure 4). It should be noted that all morphological observations were performed at constant temperature of 105 °C.

Figure 5a shows the morphology development of PS/PVME 46/54 blend, which locates in the PS-rich metastable region of the obtained phase diagram at measuring temperature. It can be seen that nucleation and growth mechanism led to the formation of spherical PVME-rich domains, which grew up with time. For the 30/70 blend which locates at unstable region, highly interconnected structure (Figure 5b) was developed at early stages of phase separation as a characteristic of spinodal decomposition. Because of the presence of highly curved interface between the two phases in the cocontinuous morphology, a considerable free energy is stored at the interface. Therefore, the microstructure is not in thermodynamic equilibrium and will break up into the droplet-matrix morphology at late stages. For 30/70 blend sample after about 50 min, interconnected structure broke up into PVME-rich droplets and PS-rich phase as a continuous matrix phase. At longer times, droplets grew dramatically, and a broad size distribution of droplets was observed. For the 10/90 blend, which locates in the PVME-rich metastable region at 105 °C, it was expected that NG mechanism led to the formation of PS-rich droplets in the PVME-rich matrix. However, it can be seen that (Figure 5c) PVME-rich droplets with no well-defined shape nucleated and started growing in size, while the PS-rich minor phase formed a continuous network structure. At longer times, phase inversion occurred, leading to breakup of the PS-rich network into disconnected domains in the PVME-rich matrix. This behavior is a characteristic of viscoelastic phase separation which takes place in the mixtures having largely different viscoelastic properties (dynamically asymmetric mixtures).

In dynamically asymmetric mixtures, domain growth induces elastic stresses in the higher viscoelastic component (the component with higher T_g) during the phase separation,[4] thereby preserving the continuity of more viscoelastic phase even when it is in the minority. This could be due to the hindering effect of induced stress on the breakup

Table 2. Investigations on PS/PVME Blend at Quench Depths Higher Than the Quench Depth Worked by Tanaka[4]

	highest quench depth (°C)	composition PS/PVME	M_w (PS)	M_w (PVME)
Voigt-Martin et al.[23]	36	40/60	54 200	75 000
Gharachorlou et al.[17]	30	40/60	248 000	110 000
Nishi et al.[24]	50	50/50	200 000	51 500

of thin polymer strands.[44−46] In the late stages of VPS, domain growth slows down, which leads to the weakening of the resulting stress fields. Hence, the network structure becomes unstable in the reduced stress field, and the interconnectivity of minor phase with higher viscoelasticity breaks into droplet-matrix morphology which is the thermodynamically favorable phase state due to lower interfacial energy.

Similar behavior was also observed for the PS/PVME 5/95 blend for which the PS-rich minor phase formed network structure and viscoelastic phase separation controlled phase behavior (not shown here in Figure 5). When the weight fraction of PS was further decreased to 3.5%, usual phase separation (thermodynamic controlled) was observed (Figure 5d) where PS-rich droplets were formed in the PVME-rich matrix by the NG mechanism. The binodal region of phase diagram determined from DSC and turbidity measurements predicted that the 3.5/96.5 PS/PVME sample was in the PVME-rich metastable region, which was supported by this morphological analysis. In other words, there was a crossover from viscoelastic to normal phase separation at critical composition of about 3.5% PS. From above results, it can be concluded that in a certain range of PS weight fraction (in this work at a range of about 3.5−10%) at constant temperature viscoelasticity can overcome thermodynamics, and hence the VPS controls phase separation behavior. In other words, in addition to the quench depth mentioned by Tanaka,[4] the occurrence of VPS strongly depends on composition of sample at a constant temperature. This explains why in some investigations on the PS/PVME blend VPS has not been observed even for deep quenches as summarized in Table 2.

It should be noted that although components with different M_w were used in the researches referred to in Table 2, the driving force for viscoelastic phase separation (the difference in the T_g's of phase separating domains[4]) at the same quench depth should be nearly the same based on Tanaka's theory.[3−5] This is due to the negligible dependence of T_g's on the molecular weight of PS and PVME for the works summarized in Table 2.

Coarsening of the phase-separating domains with time can be characterized by a power law dependence, $R \propto t^m$, where m is an exponent, depending on the coarsening mechanism. For droplet-matrix phase separation, Ostwald ripening (Lifshitz−Slyozov theory[47]) and Brownian-coagulation (Binder−Stauffer theory[48]) mechanisms are dominant. The driving force for these two mechanisms is the diffusion of material or droplets. The coarsening of the domains with time for both mechanisms is described by $m = 1/3$. For SD mechanism of phase separation, the coarsening of domains is due to the hydrodynamic flow driven by capillary forces and is described by $m = 1$ (Siggia's theory[49]). There is no theory for predicting domain size growth of network structure for sample under the VPS mechanism.

Figure 6 shows the variation of domain size with time for different phase-separating morphologies of PS/PVME blends at 105 °C obtained by image analysis of optical micrographs. The exponent m was nearly 0.35 for 3.5/96.5 PS/PVME blend, indicating diffusive type coarsening. However, it was found to be about 0.5 (more than 1/3) for the 46/54 blend, as was observed by Vinckier and Bousmina et al.[19,43] for the NG phase-separating system. This indicates a second process (in addition to the diffusion process) involved in the structure evolution. The Ostwald ripening and Brownian coagulation mechanisms ignore the interaction between droplets. Therefore, both mechanisms are valid only in the limit of low volume fractions. When the volume fraction of dispersed phase becomes higher, hydrodynamic flow fields start playing an important role that could increase the rate of droplet size change. The exponent m is nearly 1 for the 30/70 PS/PVME blend, indicating the coarsening of the domains in spinodal region is mainly driven by hydrodynamic flow mechanism, which is in agreement with the prediction of Siggia's theory. The Doi−Ohta emulsion model[31] predicts the same scaling behavior as well. The exponent m was found to be ~1.3 for sample under viscoelastic phase separation, indicating faster kinetics of phase separation in comparison to SD and NG mechanisms. This is fairly close to the scaling relationship of domain growth as $R \propto t^{3/2}$ which was obtained experimentally by Tanaka for network structure induced by viscoelastic phase separation. During the VPS, coarsening process is driven by volume shrinking of the PS-rich domains.

4.3. Rheology. *4.3.1. Linear Viscoelastic Behavior. Dynamic Frequency Sweep Experiment.* Figure 7d shows dynamic moduli, G' and G'', as a function of frequency at different phase separation times for the PS/PVME 3.5/96.5 blend which locates at the PVME-rich metastable region of the phase diagram. It can be seen that morphology evolution with phase separation time led to the development of a shoulder in the storage modulus and an increase in G' at low frequencies where $G' \propto \omega^2$ and $G'' \propto \omega$. For the 46/54 blend which locates at the PS-rich metastable region, in contrast to the 3.5/96.5 blend, G' decreased with time (corresponding to increasing the droplet size) in the metastable region (Figure 7a), and dynamic moduli exhibited a power law behavior $G' \propto \omega^n$, $G'' \propto \omega^m$ in which m and n increased with phase separation time.

The linear viscoelastic response of a polymer blend with a droplet-matrix morphology can be discussed in three different zones: (i) Low-frequency range where terminal behavior is observed $G' \propto \omega^2$, $G'' \propto \omega$. At terminal zone, the elastic contribution of the two components to G' is negligible, and the development of G' is mainly related to the interfacial tension, which in turn largely depends on the shape deformation and variation of interfacial area of the droplets formed during phase separation.[50] Therefore, G' increases with growing the droplet size during the phase separation due to the greater deformability of the larger droplets. This is consistent with Palierne's emulsion model[26] which predicts $G' \propto R$ at the terminal zone.[19] (ii) High-frequency range where the elastic contribution of the two components are dominant compared to the interfacial one; hence, the high frequency behavior of G' and G'' is not affected by the phase separation. (iii) Intermediate frequency range, where the linear viscoelastic response of a polymer blend is mainly controlled by the total interfacial area.[11] Hence, G' decreases with phase separation time due to the decreased interfacial area.

It should be noted that a certain frequency range cannot be assigned to any of above regions, since it is affected by viscoelastic properties of two phases as well as Laplace pressure. Therefore, the observed behavior of respectively increasing and decreasing G' at low frequencies by phase separation time for 96.5/3.5 and 46/54 blend samples can be explained in terms of experimentally accessible frequency range. In other words, for the 46/54 sample the observed

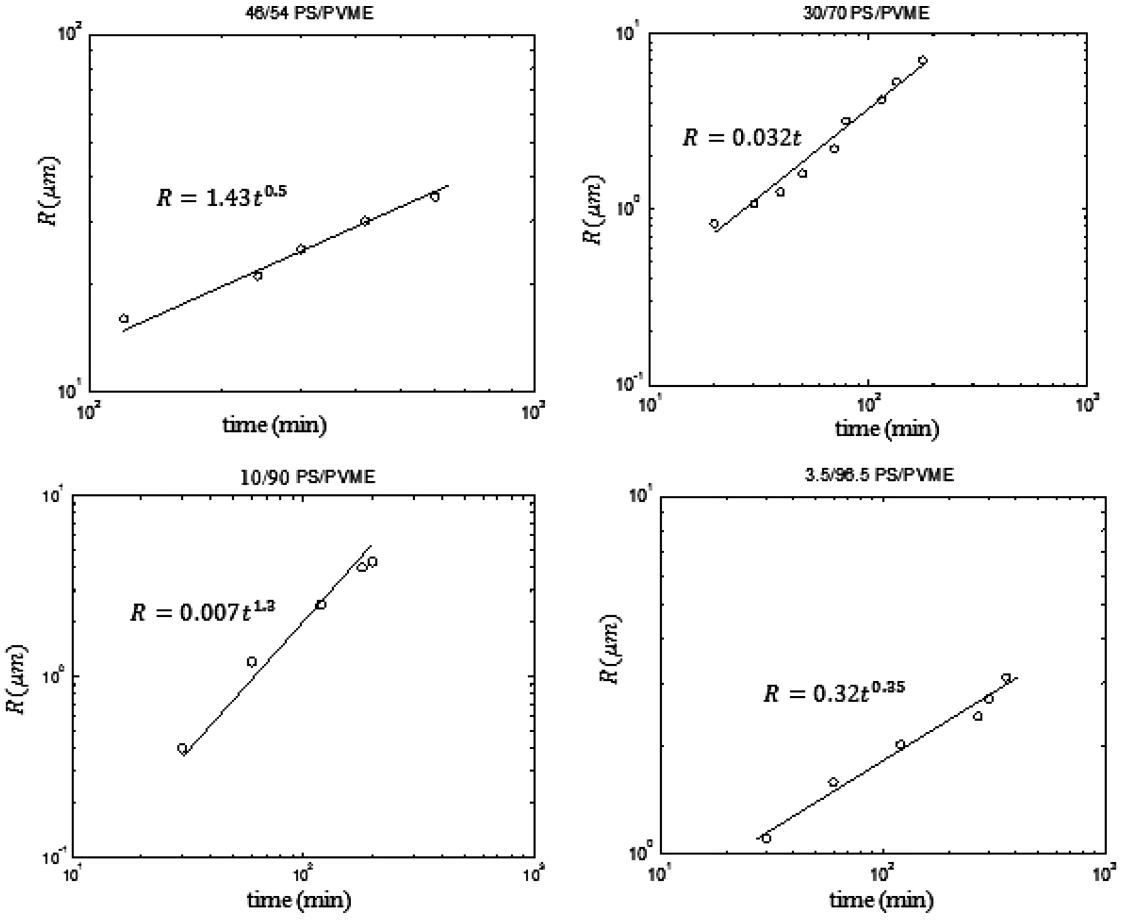

Figure 6. Variation of domain size with time for different phase-separating morphologies of PS/PVME blends at 105 °C.

behavior at low frequencies is due to the correspondence of these frequencies with intermediate frequencies at which total interfacial area is dominant, while for the 96.5/3.5 sample the observed increase of G' with phase separation time (increasing droplet size) at low frequencies is due to the correspondence of these frequencies with the experimentally accessible terminal zone at which deformability is dominant. However, it is expected that the power law behavior for 46/54 blend tends toward terminal behavior at very low frequencies. The above discussion explains the reason for inconsistencies in the literature that some researchers[19,21] observed that in the metastable region at low frequencies G' increased with time, while others observed the other way around.[10,11]

Figure 7b shows the dynamic moduli as a function of frequency at different phase separation times for the 30/70 blend for which the initial morphology was cocontinuous. It can be seen that for sample after 5 min annealing the dependence of G' and G'' on ω at low frequencies was weak, with the scaling behavior of approximately $G' \propto \omega^{0.4}$ and $G'' \propto \omega^{0.35}$. This large deviation from terminal behavior can be attributed to highly interconnected structure and high interfacial area induced by spinodal decomposition, which gave rise to dynamic moduli at low frequencies. According to the Doi−Ohta theory,[31] the elastic modulus is proportional to the interfacial area for cocontinuous morphology;[51] hence, high interfacial area induced at early stages of SD led to large increase in elastic modulus. In addition, interconnectivity in a network structure gives rise in elastic modulus according to the rubber elasticity theory.[52] Dynamic moduli decreased by time and its dependence on frequency increased as was observed by Polios et al.;[20] moreover, this behavior was preserved even after inducing droplet-matrix morphology. Decrease of the storage modulus can be understood by comparing the cocontinuous morphology with a physical network structure.[53] For a network structure, the elastic behavior is an increasing function of number of cross-links per unit volume. The interconnected structure of SD could be assumed as a network. During the coarsening process, the number of interconnections decreased and consequently the contribution of cocontinuity to G' decreased. In addition, coarsening of the structure led to decrease of interfacial area inducing a decrease in storage modulus. These arguments explain why the coarsening process during the SD resulted in decrease of storage modulus. After about 50 min from the onset of phase separation, morphology evolution led to breakup of cocontinuous structure, forming a droplet-matrix morphology; thereafter, decrease of G' during the phase separation was only a consequence of decrease in interfacial area.

Figure 7c shows dynamic moduli as a function of frequency at different phase separation times for the PS/PVME 10/90 blend in which viscoelastic phase separation controls the phase behavior. It can be seen that at early stages of phase separation, after 5 min annealing, the dependence of G' and G'' on ω at low frequencies was weak, with the scaling behavior of approximately $G' \propto \omega^{0.35}$ and $G'' \propto \omega^{0.45}$. This large deviation from terminal behavior can be attributed to the formation of PS-rich percolating network with a sponge-like pattern that hinders the flow. Self-generated stresses due to VPS led to volume shrinking of the PS-rich phase by time;[4] hence, interconnectivity of the network structure decreased until breaking up into disconnected domains. Loss of network interconnectivity induced the decrease of dynamic

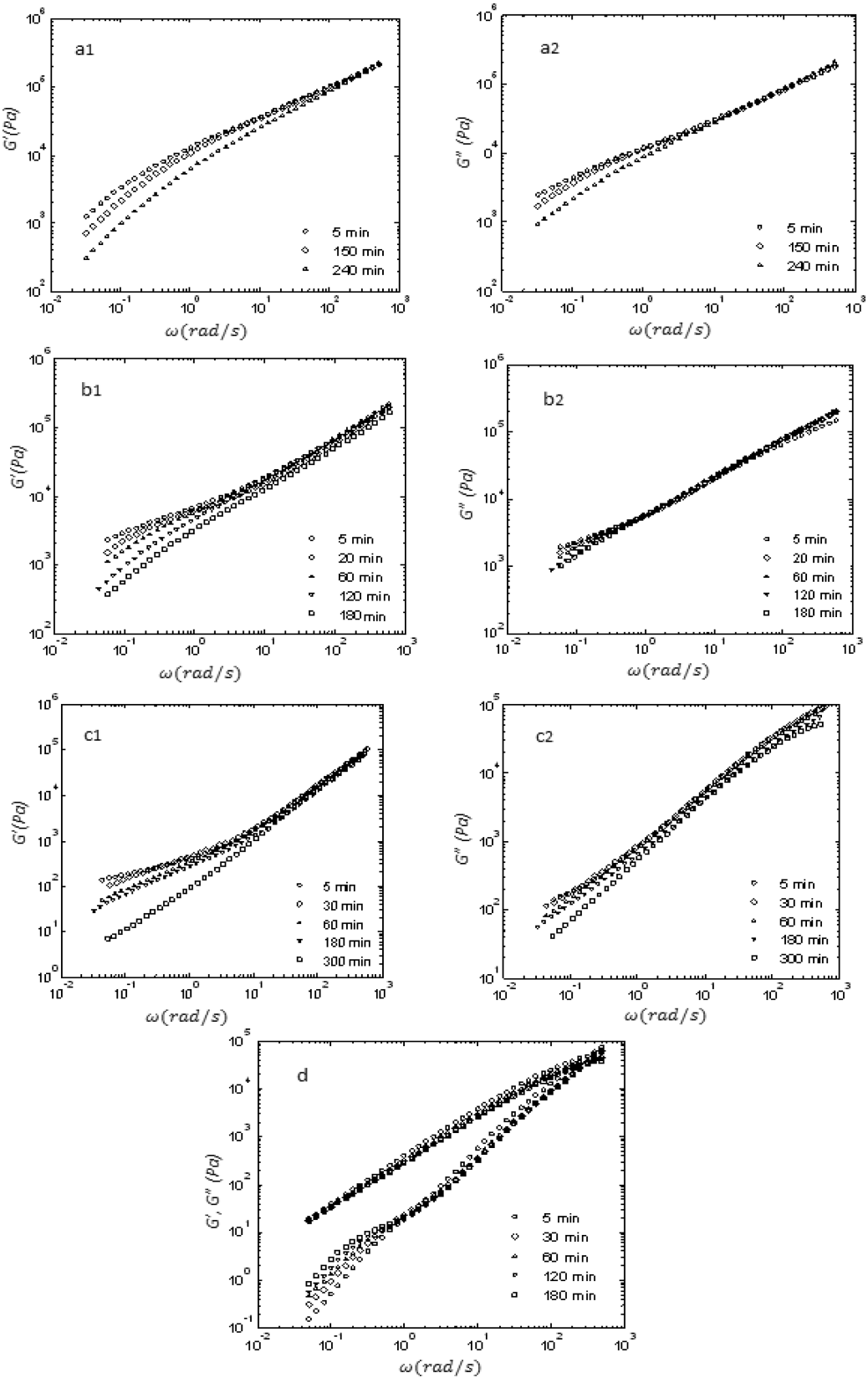

Figure 7. Dynamic moduli of PS/PVME blends at different phase separation times at 105 °C with the compositions: (a) 46/54, (b) 30/70, (c) 10/90, and (d) 3.5/96.5.

moduli at low frequencies. It is interesting to notice that for sample after 4.5 h annealing G' dramatically decreased which was due to phase inversion and breaking up the PS-rich network into disconnected domains.

tan δ vs ω. This plot can be used as a tool to differentiate the liquidlike behavior from a solidlike one. At low frequencies, the slope of tan δ curve against frequency is negative for liquids and positive for the systems with solidlike behavior.[54]

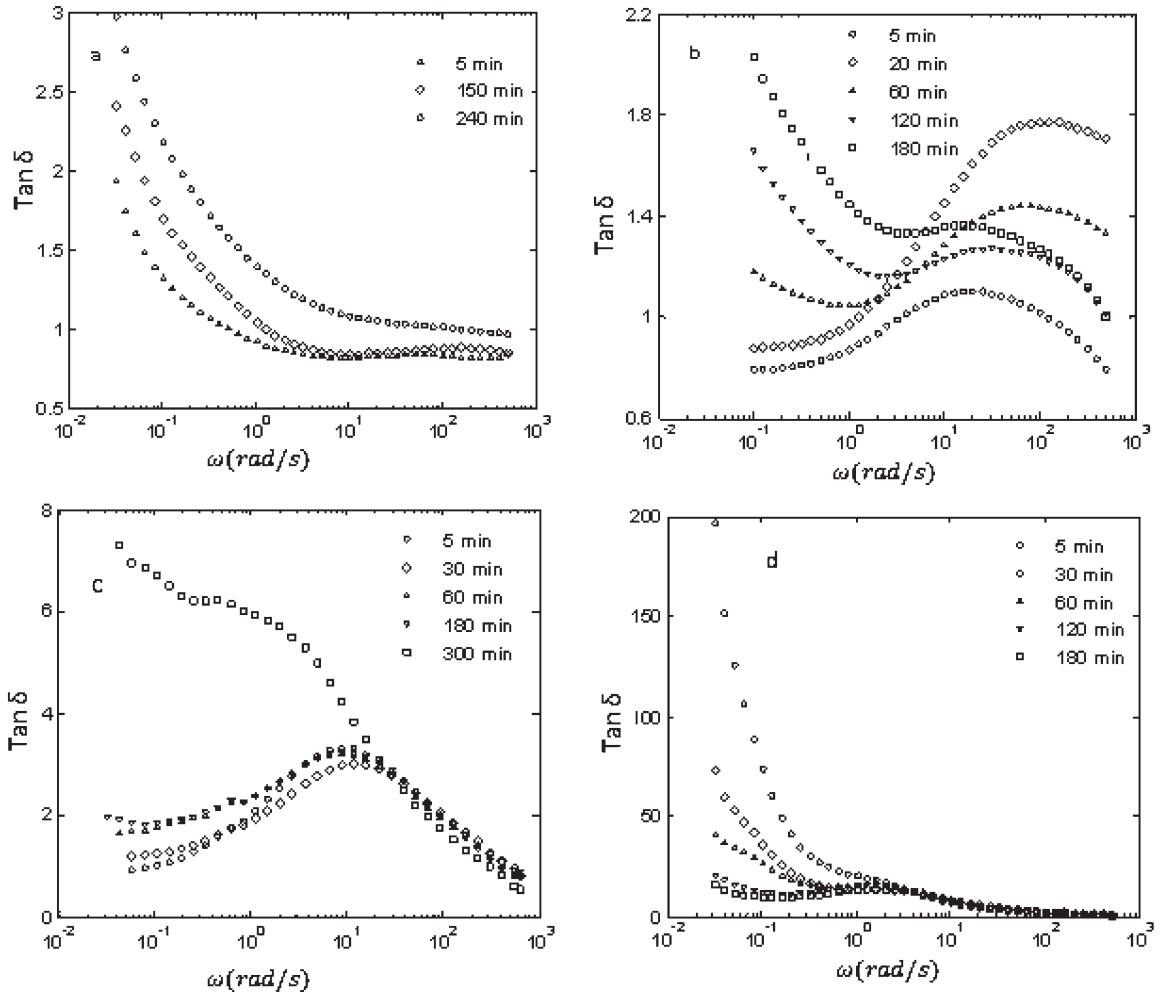

Figure 8. Plots of tan δ vs ω for PS/PVME blends at different phase separation times at 105 °C with the compositions (a) 46/54, (b) 30/70, (c) 10/90, and (d) 3.5/96.5.

Figure 8 shows the tan δ vs ω plots for PS/PVME blends at 105 °C for different phase separation times. It can be observed that regardless of matrix phase (PS-rich and PVME-rich) for samples with droplet-matrix phase separation (i.e., 3.5/96.5 and 46/54 blends), the slope of curves at low frequencies was negative at different phase separation times, indicating a fluidlike behavior. However, for the 30/70 blend, at early stages of phase separation when morphology was cocontinuous (i.e., samples with 3 and 20 min annealing), the slope of curve in the low-frequency zone was positive, indicating a solidlike behavior. This can be attributed to the interconnections of the strands of coexisting phases that can behave as strong anchor point to hinder the flow. At late stages, the slopes of curves became negative, indicating breakup of cocontinuous structure into droplet-matrix morphology.

For the 10/90 blend at early stages of phase separation, the slope at low-frequency region was negative, indicating that during the viscoelastic phase separation the system behaved as an elastic body. This is related to the self-generated stresses, which lead to formation of a network structure for PS-rich phase. This is in agreement with Tanaka's argument[4] that in addition to the initial diffusive and the final hydrodynamic regimes which are known for usual phase separation, there is an intermediate elastic regime where the elastic energy dominates phase separation, and the system behaves like an elastic gel. It should be noticed that the solidlike behavior in the spinodally decomposing sample is different from the viscoelastic phase separating one; the former is originated thermodynamically by enhancement of spinodal concentration fluctuations, while the latter has elastic origin due to the self-generated stresses induced during the phase separation. This is the reason why the spinodal decomposition can be described by the fluid model (model H in the Hohenberg−Halperin notation[55]), but such models fail to predict viscoelastic phase separation behavior.[5] To describe viscoelastic phase separation theoretically, developed models in which viscoelastic effects are incorporated may be employed.[5] As can be seen in Figure 8c, the slope in the low-frequency region after 3 h became positive for the VPS system, indicating that the system approached its final equilibrium state, where the deformation rate of domains slowed down which led to weakening of the resulting stress field. Thus, the PS-rich phase behaved like a liquid, and the system approached the phase inversion process. This critical time for phase inversion is in good agreement with the one obtained by optical microscopy.

Kinetics of Phase Separation by Rheology. To investigate phase separation kinetics under different mechanisms (NG, SD, and VPS), isothermal time sweep experiments were carried out as described in the Experimental Section. The results are shown in semilog scale in Figure 9. It can be seen that except for the 3.5/96.5 blend, G' initially increased, which is theoretically consistent with the prediction of time-dependent Ginzburg−Landau (TDGL) equation.[21] This is due to the combination effects of enhanced concentration

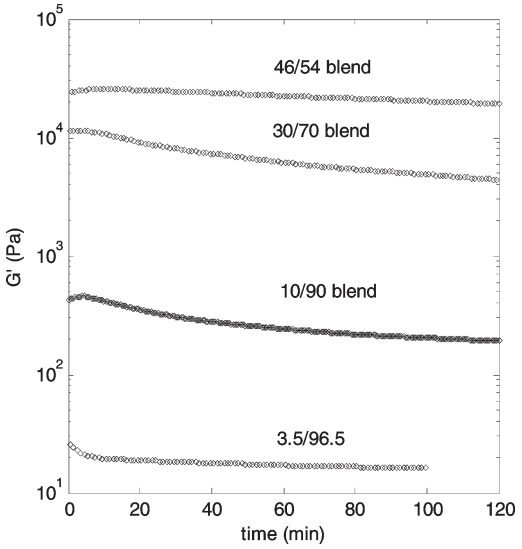

Figure 9. Time evolution of the storage modulus at frequency of 1 rad/s and given strain of 5% strain for PS/PVME blends at temperature of 105 °C.

fluctuation and induced interfacial area at early stages of phase separation. In the metastable region, the increase in interfacial area mainly contributes to the initial stress response due to the increase in volume fraction of dispersed phase, whereas the growth of concentration fluctuation plays the major role for samples under spinodal decomposition[21] and viscoelastic phase separation.[4] For the 3.5/96.5 PS/PVME blend, the initial increase in G' occurred at very early stage of phase separation (at the first 30 s of time sweep experiment), which was not picked up by time sweep experiment. After saturation of concentration fluctuations, the interfacial area per unit volume decreased which induced a decrease of G' due to the interfacial tension-driven coarsening of phase domains (in cocontinuous system), coalescence and Ostwald ripening (in the droplet-matrix system), or volume shrinking of PS-rich phase (in VPS).

It can be seen that for samples phase separating by NG (46/54 and 3.5/96.5 blends), the phase separation process was slower and weaker than those phase separating by SD (30/70 blend) and VPS (10/90 blend). This in agreement with the scaling relationships obtained in section 4.2. For the 10/90 blend for which VPS controls phase-separation process, G' dramatically decreased with phase separation time, reflecting the fast growth of the PVME-rich droplets. This is in agreement with the scaling relationship of domain growth as $R \propto t^{1.3}$ obtained in section 4.2, indicating faster kinetics of phase separation in comparison to SD and NG mechanisms. After enhancement of the concentration fluctuations at early stages of viscoelastic phase separation, domain shape is governed by viscoelastic stresses, while the interfacial tension plays a minor role. During the VPS, the coarsening process was driven by volume shrinking of the PS-rich domains,[4] which led to loss of connectivity of the PS-rich network, inducing decrease of G'. It should be noted that the results of time sweep experiments were consistent with the frequency sweep ones. In the frequency sweep experiments, G' also decreased with phase separation time at frequency of 1 rad/s, which was far from the terminal zone.

4.3.2. Modeling Linear Viscoelastic Behavior

Fundamentals. The purpose of this section is to examine the ability of Palierne's emulsion model[26] to describe linear viscoelastic properties of phase-separating PS/PVME blends. This model has been originally developed for completely immiscible blends. For uncompatibilized polymer blends, and when the droplets polydispersity is less than 2.3, Palierne's emulsion model predicts the complex modulus of the mixture, $G^*(\omega)$, as follows:[25]

$$G^* = G_m^* \frac{1 + 3\varphi_d H^*}{1 - 2\varphi_d H^*} \tag{10}$$

where

$$H^* = \frac{4(\alpha/R)[2G_m^* + 5G_d^*] + [G_d^* - G_m^*][16G_m^* + 19G_d^*]}{40(\alpha/R)[G_m^* + G_d^*] + [2G_d^* + 3G_m^*][16G_m^* + 19G_d^*]} \tag{11}$$

where the subscripts "m" and "d" refer to the matrix and dispersed phase, respectively; α is the interfacial tension, φ_d is the volume fraction of the dispersed phase, and R is the volume average radius of dispersed droplets. Because a phase-separating blend with composition ϕ consists of PS-rich and PVME-rich domains, the composition of each phase domain (ϕ' and ϕ'') was determined by the tie line of phase diagram at 105 °C. Then, the volume fraction of the dispersed phase, φ_d, was calculated by a conservation equation as follows:[56]

$$\phi = \varphi_d \phi' + (1 - \varphi_d)\phi'' \tag{12}$$

This equation can be rearranged to obtain the volume fraction of dispersed phase as follows:

$$\varphi_d = \frac{\phi - \phi''}{\phi' - \phi''} \tag{13}$$

Thus, the only undefined parameter in Palierne's emulsion model is Laplace pressure, α/R; however, R can be determined from optical micrographs, and the interfacial tension α was obtained by rheological measurements as discussed in the following section.

To apply Palierne's model, phase separation process should be reached to the late stage of phase separation at which phase-separating domains have attained their equilibrium concentration profile. For the 30/70 blend, the model was applied after breaking up of the cocontinuous domains into droplet-matrix morphology, which occurred in the late stage of phase separation. For 3.5/96.5 and 46/54 blends, which located in the binodal region, according to the time sweep results, initial increase of storage modulus, corresponding to the early stage of phase separation, occurred at times less than 5 min. Therefore, after 1 h of phase separation, the blend was already in the late stages of phase separation, as was shown by Kim et al.,[22] and hence Palierne's model can be applied.

Evaluation of Interfacial Tension. In this section, the interfacial tension of PS/PVME blend was calculated from rheological measurements based on relaxation time of interface. For this purpose, the PS/PVME 3.5/96.5 blend was chosen for which storage modulus reached the terminal zone at low frequencies, as was shown earlier (Figure 7d). At the terminal zone, development of the storage modulus is mainly related to shape recovery of the droplets due to the interfacial tension.[50]

Figure 10 shows the weighted relaxation time spectrum, $\tau \times H(\tau)$, as a function of relaxation time, τ, at different phase separation times for the 3.5/96.5 blend. As can be seen, the blend spectrum exhibited two maxima. The first one coincided with that of the matrix, PVME-rich phase, suggesting that the matrix governs the rheological behavior of the blend at high frequencies. The second peak detected at longer

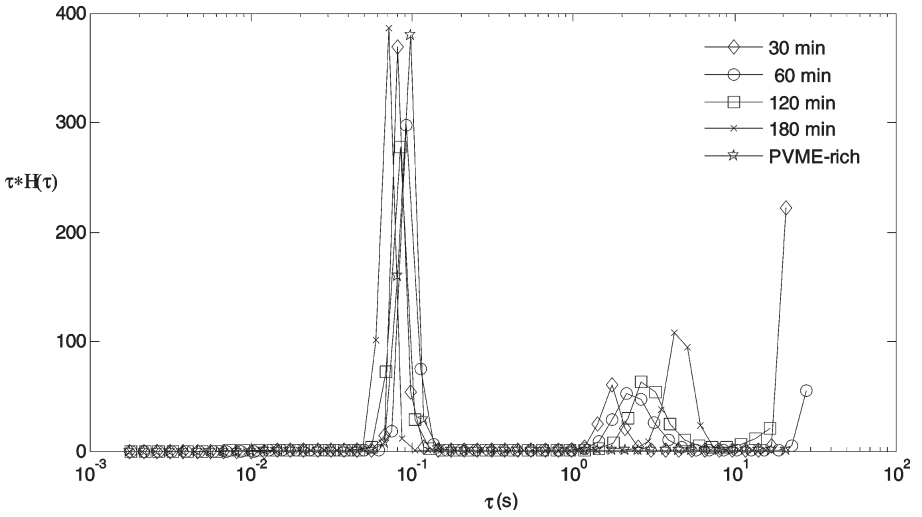

Figure 10. Weighted relaxation spectra of the PS/PVME 3.5/96.5 blend at 105 °C.

relaxation times is associated with the shape relaxation of the droplets. As the dispersed phase size increased, the second peak shifted toward longer times (i.e., increase of the relaxation time).

The relaxation time of interface for droplet-matrix morphology can be expressed by the following equation given by Palierne's model:[25]

$$\tau = \frac{R\eta_m}{4\alpha}\frac{(19k+16)[2k+3-2\varphi_d(k-1)]}{10(k+1)-2\varphi_d(5k+2)} \qquad (14)$$

where k is the viscosity ratio of the dispersed phase to the matrix. From Figure 10, relaxation time of the droplets for the 3.5/96.5 blend after 30 min annealing was obtained as 2.1 s, and hence by using the eq 14, interfacial tension was calculated to be 0.056 mN/m. The obtained interfacial tension is very close to the one reported in the literature[43] for the same system.

It should be mentioned that the other blend samples (46/54, 30/70, and 10/90) have not been examined here because the terminal behavior, corresponding to the relaxation of interface, was not observed in the studied frequency range (as is shown in Figure 7). In other words, the characteristic peak of interface was not appeared in the variation of $\tau \times H(\tau)$ against τ for further analysis.

Comparison with Palierne's Emulsion Model. Figure 11 compares the experimental results and theoretical predictions of storage modulus as a function of frequency for different phase-separating PS/PVME blends with droplet-matrix morphologies at 105 °C. It should be noticed that for the 30/70 blend after about 50 min annealing breaking up of structure led to formation of droplet-matrix morphology; hence, Palierne's emulsion model can be applied.

Figure 11c shows that there is a good agreement between the experimental results and theoretical predictions for the 3.5/96.5 blend for which morphology was PS-rich droplets in PVME-rich matrix. The predictions of Palierne's model were obtained by using $R = 1.7$ and 2 μm for samples after 120 and 180 min annealing, respectively. However, for 30/70 and 46/54 blends with the morphology of PVME-rich droplets dispersed in the PS-rich matrix, Palierne's model predicted higher values than the experimental results and the deviation increased with phase separation time. Similar behavior was reported by Kapnnistos et al.[15] for the PS/PVME phase-separating blend. The predictions of Palierne's model for the 30/70 blend were obtained by using $R = 4$ and 6 μm for samples after 120 and 180 min annealing, respectively, and for the 46/54 blend by $R = 18$ and 23 μm for samples after 150 and 240 min annealing, respectively.

As seen, Palierne's model predicted higher values than experimental data for morphologies of PVME-rich droplets dispersed in the PS-rich matrix phase. This deviation was more pronounced at longer times of phase separation at which PVME-rich droplets were bigger in size. This is likely related to the self-generated stresses in the PS-rich matrix phase. As mentioned earlier, during the phase separation, growth of the PVME-rich droplets can induce viscoelastic stresses in the PS-rich matrix phase. As the stress in entangled polymer systems is supported by molecules, a stress gradient would create a net force on the chains, resulting in their relative migration and increasing the chain mobility which in turn allows polymer chains to flow.[57,58] Since in mixtures with droplet-matrix morphology rheological behavior is mainly controlled by matrix phase, stress-enhanced mobility in the matrix phase, which is not considered in the classic Palierne model, leads to a large difference between experimental and theoretical results.

The stress-enhanced mobility may be compensated by replacing the dynamic moduli of PS-rich phase with those obtained at higher temperatures than 105 °C (typically, 105 + ΔT °C, where an increase of ΔT °C is considered). But, it is clear that at temperatures higher than 105 °C the corresponding PS-rich mixture is located in the two-phase region. In other words, since the rheological properties of the PS-rich single phase at higher temperatures than phase separation limit cannot be measured experimentally, an alternative method should be used to obtain such results. Thus, we extrapolated dynamic moduli of PS-rich phase at higher temperatures by applying the double-reptation mixing rule proposed for miscible blends which is known to give adequate prediction.[59−61] Lee et al. simplified the double-reptation mixing rule as follows:[61]

$$G_1'(\omega) = \phi_1^2 G_1'(\omega) + \frac{8G_1'(\omega)G_2'(\omega)\phi_1\phi_2}{G_1'(\omega)+2\sqrt{G_1'(\omega)}\sqrt{G_2'(\omega)}+G_2'(\omega)} + \phi_2^2 G_2'(\omega) \qquad (15)$$

$$G_1'' = \phi_1^2 G_1''(\omega) + \frac{4G_1'(\omega)G_2'(\omega)\phi_1\phi_2}{G_1'(\omega)+G_2'(\omega)} + \phi_2^2 G_2''(\omega) \qquad (16)$$

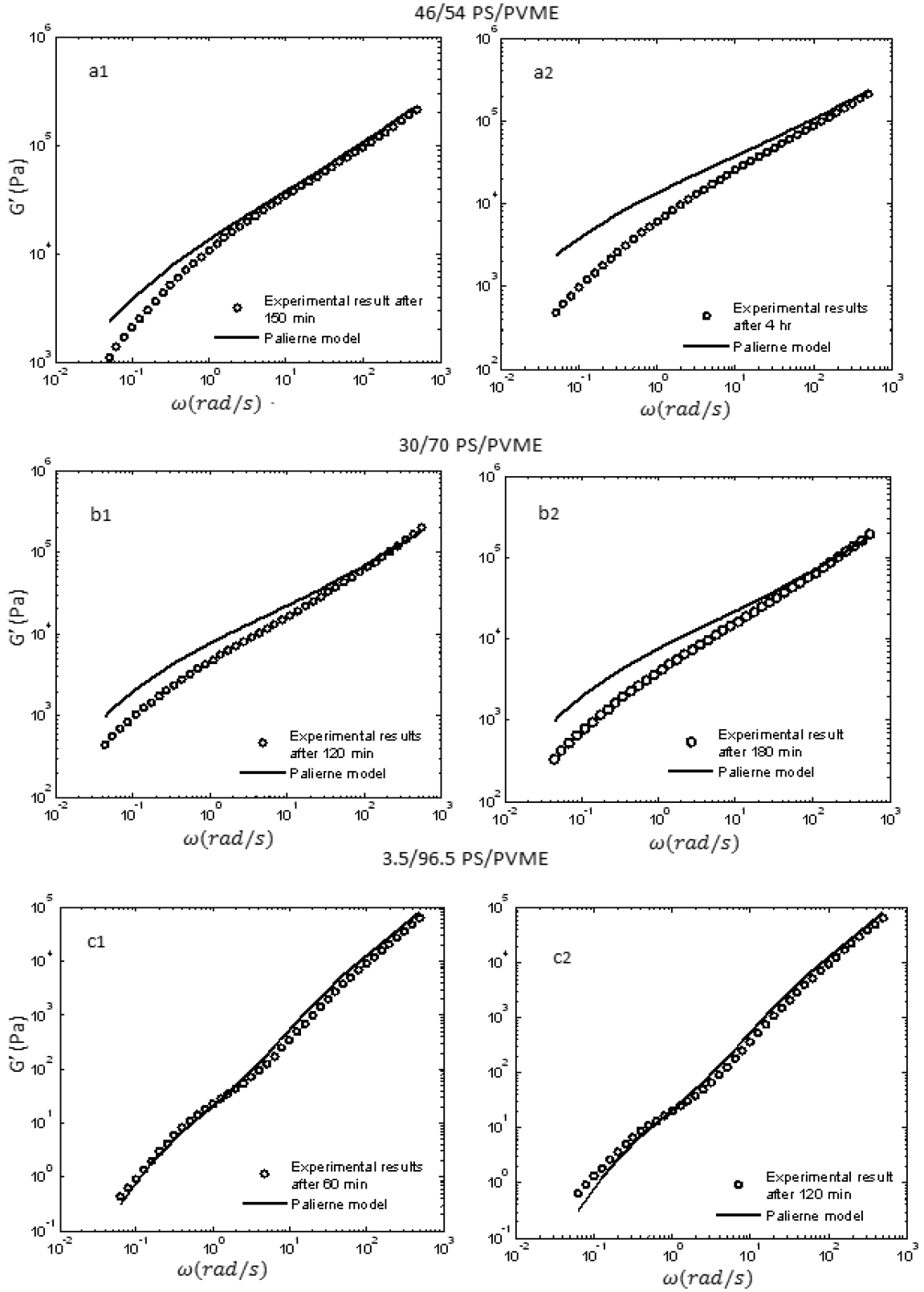

Figure 11. Comparison between experimental storage modulus and predictions of Palierne's model for PS/PVME blends at different phase separation times at 105 °C.

where ϕ_1 and ϕ_2 are volume fractions of polymer 1 and 2 in component 1-rich phase. The double-reptation mixing rule assumes that the two components have similar glass transition temperature (T_g). When the T_g's of two components are dramatically different, the monomeric frictions of the components in mixed state are different from those in the pure state at the identical temperature.[62,63] This difference arises from the change of effective glass transition temperature of components in the mixture. In other words, the PS and PVME molecules in the PS-rich phase have a different glass transition temperatures, $T_{g_{eff}}$, from pure PS and PVME molecules, respectively. Lee et al.[61] proposed a model to

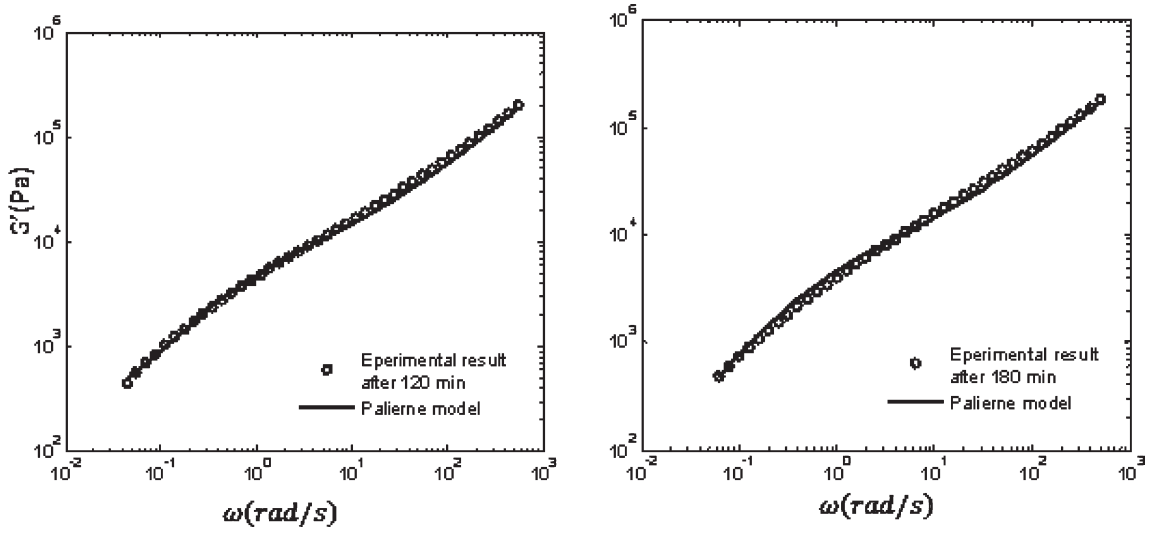

Figure 12. Comparison between experimental storage modulus of 30/70 blend at 105 °C and prediction of Palierne's model by using dynamic moduli of PS-rich phase at temperatures of (a) 105 + 7.5 °C and (b) 105 + 10 °C.

compensate this difference by using an effective glass transition temperature. Therefore, based on the Lee et al. model, the dynamic moduli of each component in eqs 15 and 16 should be taken from the results obtained at the adjusted temperature $T_{adj} = T_{g_{eff}} + dT$, where the dT is the difference between measuring temperature, T, and T_g of pure polymer chains ($T_{adj} = T + T_{g_{eff}} - T_g$). $T_{g_{eff}}$ of each component can be obtained as follows:[63]

$$T_{gA_{eff}}(\phi_1) = T_{g2} + (T_{g1} - T_{g2})[(1 + K_1)\phi_{1_{eff}} - (K_1 + K_2)\phi_{1_{eff}}{}^2 + K_2\phi_{1eff}{}^3] \quad (17)$$

where $T_{g1_{eff}}$ is the $T_{g_{eff}}$ of polymer 1; T_{g1} and T_{g2} are respectively the glass transitions of pure polymers 1 and 2; K_1 and K_2 are parameters which are −0.707 and 0.462 for the PS/PVME blend, respectively;[64] and $\phi_{1_{eff}}$ is the effective local concentration of polymer 1 in the blend which can be obtained from following equation:[63]

$$\phi_{1eff} = \phi_s + (1 - \phi_s)\phi_1 \quad (18)$$

where ϕ_s is the self-concentration term whose magnitudes for PS and PVME are 0.27 and 0.25, respectively.[63]

To obtain the best temperature for good agreement between the prediction of Palierne's model and the experimental result, the G' and G'' of PS-rich phase were extrapolated by double-reptation model, eqs 15−18, at different temperatures higher than 105 °C. A good agreement between the experimental results and theoretical predictions of the 30/70 blend after 120 and 180 min annealing was obtained by extrapolating the dynamic moduli of PS-rich phase to the temperatures of 105 + 7.5 °C and 105 + 10 °C, respectively (Figure 12). In other words, considering the effect of self-generated stresses in the PS-rich matrix can be used to compensate the overestimation of Palierne's model for the PS/PVME dynamically asymmetric blend. These results suggest that studying rheology of phase-separating blends (partially miscible) is rather complex because not only the phase separation process (the interplay between thermodynamics and kinetics) but also the effect of viscoelasticity on the phase separation should be taken into account. It is therefore clear that for an accurate theoretical prediction incorporating details of the phase separation process into the emulsion models is essential.

4.3.3. Transient Shear Flow Behavior

Start-up Shear Flow Response. In start-up shear flow experiments, a constant shear rate is imposed on a sample which is initially at rest and equilibrium. It is known that shear flow can induce mixing or demixing depending on magnitude of imposed shear rate.[8,9] However, the stress overshoot in most of the start-up shear flow experiments in this work occurred within the first 60 s of the measurement, and the selected shear rate, 0.2 s^{-1}, was too low to affect the phase diagram.[8] At such low strains, the effect of phase separation on the morphology is insignificant (mixing/demixing process is negligible), and it was shown that the nonlinear behavior is mainly due to the initial induced morphology.[30,32]

Figure 13 shows the results of normalized transient shear stress in start-up shear flow experiments for samples with different phase separation times. For the 46/54 blend at different phase separation times, a stress overshoot typical of nonlinear viscoelastic behavior was observed at short times, followed by a steady state region (Figure 13a). For this sample which had droplet-matrix morphology, the stress overshoot was attributed to the deformation of the droplets into an ellipsoidal shape with the major axis oriented with an angle, θ, with respect to the flow direction. For small deformations, θ is close to 45°; while for large deformations, θ becomes smaller than 45°, and deformed droplet becomes more oriented in the flow direction.[28,29]

It can be seen that for the 46/54 blend, with increasing phase separation time, which corresponds to the increase of droplet size, the magnitude of stress overshoot increased. This can be attributed to tendency of the larger droplets to be more deformed and then oriented toward the flow direction. This trend can be predicted by the Cheffery−Brenner model,[65] which gives the value of steady-state orientation angle. This model, which is known to give adequate prediction,[66] is as follows:

$$\theta = \frac{\pi}{4} - \frac{(19k + 16)(2k + 3)}{80(k + 1)} Ca \quad (19)$$

where Ca is the capillary number. According to this equation, for small values of Ca (small droplets or low shear rates) the orientation angle is close to 45°; however, with increasing the Ca (larger droplets or higher shear rates), droplets tend to be more oriented toward the flow direction.

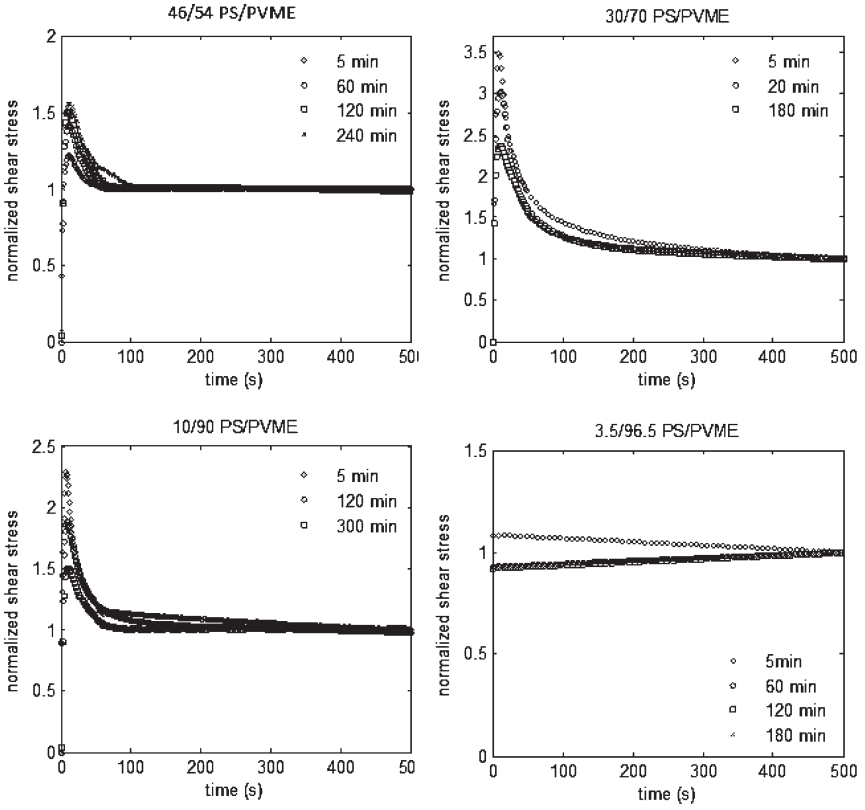

Figure 13. Normalized stress growth at shear rate of 0.2 s^{-1} and 105 °C for PS/PVME blends.

The 30/70 blend sample, which located in unstable region, exhibited a strong stress overshoot at early stages of phase separation, and in contrast to the 46/54 blend sample, stress overshoot decreased with phase separation time (Figure 13b). For this sample having cocontinuous morphology, the stress overshoot can be attributed to the stretching and/or orientation of the cocontinuous domains.[30] The strong overshoot at early stages of phase separation can be attributed to the highly interconnective structure with a large interfacial area. According to the Doi−Ohta[31] theory, higher interfacial area induces larger stress overshoot. Moreover, interconnectivity in a structure leads to stress overshoot.[32] Hence, the decrease of stress overshoot for samples with longer annealing in the spinodal decomposition regime can be explained by decrease of interconnectivity and interfacial area due to the coarsening process.

The 10/90 blend exhibited a strong overshoot at early stages of phase separation which decreased with phase separation time. The pronounced stress overshoot can be attributed to the percolated network structure of viscoelastic phase separating sample. According to the dynamic equations derived based on time-dependent Ginzberg−Landau model,[32] for a percolated network induced during VPS, the strong overshoot is mainly due to network deformation under shear, indicating that the PS-rich phase behaved like a percolated gel and mainly supported the applied stress. The volume shrinking of the PS-rich phase during the VPS by time led to the decrease of interconnectivity and hence decrease of stress overshoot magnitude. In the case of the 3.5/96.5 blend, for which the morphology was PS-rich droplets in PVME-rich matrix, no stress overshoot can be observed at different phase separation times (Figure 13d). This could be due to the very low volume fraction of dispersed phase as well as the highly viscous dispersed phase which cannot be deformed.

These results indicate that the stress growth behavior upon start-up of shear flow, similar to the linear viscoelastic one, is strongly dependent on the morphology of sample and correlated well with the evolution of the phase-separating morphologies.

4.3.4. Modeling Start-up Shear Flow. The aim of this section is to compare the experimental results of start-up shear flow experiments with the predictions of theoretical models. Generally, to predict the total stress, contribution of the interfacial stresses should be added to the stress resulting from the components. Contribution of the interfacial stresses can be obtained from Doi−Ohta[31] or Bousmina[28] theories. To calculate the contribution of the components to total stress, Lacroix's approach in using Palierne's model[67] can be employed, which is known to provide adequate prediction.[29] This model is developed for droplet-matrix morphology as follows:

$$\sigma_{ij}^{\mathrm{bulk}} = \eta_{\mathrm{m}}\dot{\gamma}_{ij}\left(\frac{1+1.5H}{1-H}\right) \tag{20}$$

$$H = \varphi_{\mathrm{d}}\frac{2(\eta_{\mathrm{d}}-\eta_{\mathrm{m}})}{2\eta_{\mathrm{d}}+3\eta_{\mathrm{m}}} \tag{21}$$

Figure 14 presents the result of shear start-up experiment for the 30/70 blend after 3 h annealing with the prediction of Palierne's model. It can be seen that the model predicts higher stresses than the experimental values, while the theoretical curve was obtained without considering the interfacial contribution, which clearly increases the deviation between the experimental result and theoretical one.

Recall that in the Linear Viscoelastic Behavior section, Palierne's emulsion model predicted higher values than experimental results, which was attributed to the stress-enhanced mobility due to the self-generated stresses during the phase separation. It was shown that for the 30/70 blend after 3 h annealing extrapolating the viscoelastic properties

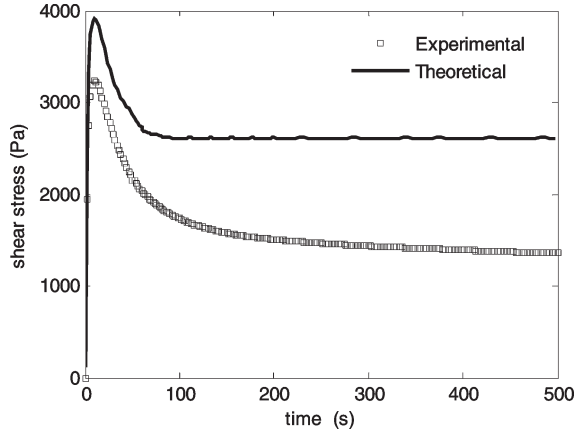

Figure 14. Comparison of experimental data of 30/70 after 180 min annealing and prediction of Palierne's model (shear rate 0.2 s^{-1}, T = 105 °C).

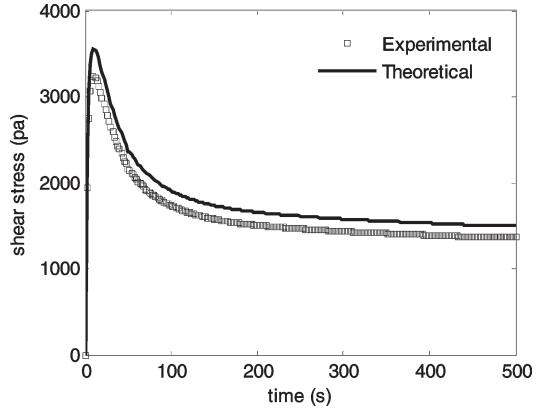

Figure 15. Comparison between experimental stress growth result of 30/70 blend at 105 °C after 3 h annealing with prediction of the Palierne's model by using viscoelastic properties of PS-rich phase at temperature of 105 + 10 °C (shear rate 0.2 s^{-1}).

of PS-rich sample to 105 + 10 °C (i.e., 10 °C increase in temperature) can compensate the effect of self-generated stresses and resulted in proper prediction of Palierne's model.

Similarly, the difference between result of shear start-up experiment and Palierne's model can be attributed to the stress-enhanced mobility due to the self-generated stresses in the PS-rich phase. As was mentioned in the Linear Viscoelastic Behavior section, the rheological properties of PS-rich phase was obtained at temperature of 105 + 10 °C by using the mixing rules proposed for miscible blends to compensate self-generated stresses. Thus, a linear mixing rule (eq 22), which was obtained for polymers with same elasticity,[68] was used.

$$\sigma = (\phi\sigma_d + (1-\phi)\sigma_m) \qquad (22)$$

To use this linear mixing rule for PS and PVME for which elastic properties are significantly different, the same procedure mentioned in section 4.3.2 was employed.

Theoretical results obtained by this procedure for the 30/70 blend after 3 h annealing, beside experimental data, are shown in Figure 15. It can be seen that theoretical model still predicts higher values than experimental data even without considering the interfacial contribution. This is maybe due to the external flow which can increase the effect of enhanced mobility in the PS-rich phase. In a blend, with a large difference in the viscoelastic properties of the components, the applied stress is mainly supported by the more elastic component (here PS-rich phase).[32]

5. Conclusion

In this work, we studied the correlation between the evolutions of different phase-separating morphologies and corresponding linear rheological behaviors as well as stress growth response upon start-up of shear flow for PS/PVME blends both experimentally and theoretically. The effect of viscoelasticity on the phase separation behavior was also examined. It was found that in addition to the quench depth at a constant temperature proposed by Tanaka[4] occurrence of VPS was strongly dependent on the composition of samples, and explicitly in a certain range of PS weight fraction (about 3.5−10% in this work), viscoelasticity overcame thermodynamics and VPS controlled phase separation behavior.

Both linear and nonlinear rheological behaviors of different phase-separating PS/PVME blends consistently correlated well with the evolution of the corresponding phase-separating morphologies. For blends phase separating by NG mechanism, deformability of the droplets mainly controlled the linear viscoelastic and stress growth behaviors; while high interfacial area and high interconnectivity of sample under SD and percolation of PS-rich phase in sample with VPS mechanism controlled the rheological behavior. Both cocontinuous morphology induced by SD and percolated network structure induced by VPS exhibited solidlike behavior; however, the rheological behavior of the former originated thermodynamically by enhancement of spinodal concentration fluctuation, while the solidlike behavior of the latter had an elastic origin due to the self-generated stresses induced during the phase separation. Time sweep experiments of elastic modulus, G', showed that the viscoelastic stresses induced by VPS led to faster kinetics of phase separation in comparison to the samples phase separating by NG and SD mechanisms.

Rheological behaviors were compared with predictions of Palierne's model. This model predicted higher than the experimental results which was attributed to the self-generated stresses induced during the phase separation in the matrix phase. An attempt was made to include these self-generated stresses in the models, which resulted in satisfactory predictions.

Acknowledgment. We thank Mrs. Tahereh Samaee Yekta for her assistance in carrying out the morphological observations of this work.

References and Notes

(1) Tanaka, H. *Adv. Mater.* **2009**, *21*, 1872–1880.
(2) Ahluwalia, R. *Phys. Rev. E* **1999**, *59*, 263–268.
(3) Tanaka, H.; Araki, T. *Macromolecules* **2001**, *34*, 1953–1963.
(4) Tanaka, H. *Phys. Rev. Lett.* **1996**, *76*, 787–790.
(5) Tanaka, H. *Phys. Rev. E* **1997**, *56*, 4451–4462.
(6) Balsara, N. P.; Rappl, T. J.; Lefebvre, A. A. *J. Polym. Sci., Part B: Polym. Phys.* **2004**, *42*, 1793–1809.
(7) Patel, A. J.; Balsara, N. P. *Macromolecules* **2007**, *40*, 1675–1683.
(8) Mabrouk, K. E.; Bousmina, M. *Polymer* **2005**, *46*, 9005–9014.
(9) Takahashi, Y.; Suzuki, H.; Nakagawa, Y.; Noda, I. *Macromolecules* **1994**, *27*, 6476–6481.
(10) Niu, Y.; Yang, L.; Shimizu, K.; Pathak, J. A.; Wang, H.; Wang, Zh. *J. Phys. Chem. B* **2009**, *113*, 8820–8827.
(11) Niu, Y. H.; Wang, Z. G. *Macromolecules* **2006**, *39*, 7175–4183.
(12) Zhang, R.; Cheng, H.; Zhang, C.; Sun, T.; Dong, X.; Han, C. *Macromolecules* **2008**, *41*, 6818–6829.
(13) Ajji, A.; Choplin, L. *Macromolecules* **1991**, *24*, 5221–5223.
(14) Fredrickson, G. H.; Larson, R. G. *J. Chem. Phys.* **1987**, *86*, 1553–1560.
(15) Kapnistos, M.; Vlassopoulos, D.; Anastasiadis, S. H.; Stammer, A.; Wolf, B. A. *Macromolecules* **1996**, *29*, 7155–7163.

(16) Sharma, J.; Clarke, N. *J. Phys. Chem. B* **2004**, *108*, 13220–13230.
(17) Gharachorlou, A.; Goharpey, F. *Macromolecules* **2008**, *41*, 3276–3283.
(18) Bousmina, M.; Lavoie, A.; Riedl, B. *Macromolecules* **2002**, *35*, 6274–6283.
(19) Vinckier, I.; Laun, H. M. *Rheol. Acta* **1999**, *38*, 274–286.
(20) Polios, I. S.; Soliman, M.; Lee, C.; Gido, S. P.; Roher, S. K.; Winter, H. H. *Macromolecules* **1997**, *30*, 4470–4480.
(21) Zhang, Z. L.; Zhang, H. D.; Yang, Y. L.; Vinckier, I.; Laun, H. M. *Macromolecules* **2001**, *34*, 1416–1429.
(22) Kim, J. K.; Son, H. W.; Lee, Y.; Kim, J. *J. Polym. Sci., Part B: Polym. Phys.* **1999**, *37*, 889–906.
(23) Voiget-Martin, I. G.; Leister, K, H.; Resenau, R.; Koningsveld, R. *J. Polym. Sci., Part B: Polym. Phys.* **1986**, *24*, 723–751.
(24) Nishi, T.; Wang, T. T.; Kwei, T. K. *Macromolecules* **1975**, *8* (2), 227–234.
(25) Graebling, D.; Muller, R.; Palierne, J. F. *Macromolecules* **1993**, *26*, 320–329.
(26) Palierne, J. F. *Rheol. Acta* **1990**, *29*, 204–214.
(27) Friedrich, C.; Gleinser, W.; Korat, E.; Maier, D.; Weese, J. *J. Rheol.* **1995**, *39*, 1411–425.
(28) Bousmina, M.; Aouina, M.; Chaudhry, B.; Guenette., R.; Bretas, R. *Rheol. Acta* **2001**, *40*, 538–551.
(29) Macaubas, P. H. P.; Demarquette, N. R.; Dealy, J. M. *Rheol. Acta* **2005**, *44*, 295–312.
(30) Krishnan, K.; Burghardt, W. R.; Lodge, T. P.; Bates, F. S. *Langmuir* **2002**, *18*, 9676–9686.
(31) Doi, M.; Ohta, T. *J. Chem. Phys.* **1991**, *95*, 1242–1248.
(32) Imaeda, T.; Furukawa, A.; Onuki, A. *Phys. Rev. E.* **2004**, *56*, 4451–4462.
(33) Chopra, D.; Vlassopoulos, D.; Hatzikiriakos, S. G. *J. Rheol.* **2000**, *44*, 27–45.
(34) Han, C. C.; Okada, M.; Muroga, Y.; McCrackin, F. L.; Bauer, B. J.; Tran-Cong, Q. *Polym. Eng. Sci.* **1986**, *26*, 3–8.
(35) Rinaldi, P. L.; Wagler, T.; Han, C. D.; Chun, H. *Macromolecules* **2000**, *33*, 1778–1789.
(36) Mabrouk, K. E.; Bousmina, M. *Rheol. Acta* **2006**, *45*, 959–969.
(37) Perti, H. M.; Stammer, A.; Wolf, B. A. *Macromol. Chem. Phys.* **1995**, *196*, 1453–1463.
(38) Reich, S.; Cohen, Y. J. *J. Polym. Sci., Polym. Phys. Ed.* **1981**, *19*, 1255–1267.
(39) Wolf, B. A. *Macromolecules* **1984**, *17*, 615–618.
(40) Kim, J. K.; Lee, H. H.; Son, H. W.; Han, C. D. *Macromolecules* **1998**, *31*, 8566–8578.
(41) Richardson, M. J.; Savill, N. G. *Polymer* **1977**, *18*, 3–9.
(42) Stadler, P. F.; Feitas, L. L.; Krieger, V.; Klotz, S. *Polymer* **1988**, *29*, 1643–1647.
(43) Mabrouk, K. E.; Bousmina, M. *Rheol. Acta* **2006**, *45*, 877–889.
(44) Goldin, M.; Yerushalmi, H.; Pfeffer., R.; Shinnar, R. *J. Fluid Mech.* **1969**, *38*, 689–711.
(45) Bousfield, D. W.; Keunings, R.; Marrucci, G.; Denn, M. M. *J. Non-Newtonian Fluid Mech.* **1986**, *21*, 79–97.
(46) Larson, R. G. *Rheol. Acta* **1992**, *31*, 213–263.
(47) Lifshitz, I. M.; Slyozov, V. V. *J. Phys. Chem. Solids* **1961**, *19*, 35–50.
(48) Binder, K.; Stauffer, D. *Phys. Rev. Lett.* **1974**, *33*, 1006–1009.
(49) Siggia, E. D. *Phys. Rev. A* **1979**, *20*, 595–605.
(50) Lacroix, C.; Grmela, M.; Carreau, P. J. *J. Rheol.* **1998**, *42* (1), 41–62.
(51) Vinckier, I.; Laun, H. M. *J. Rheol.* **2001**, *45* (6), 1373–1385.
(52) Treloar, L. R. G. *The Physics of Rubber Elasticity*, 3rd ed.; Clarendon Press: Oxford, 1975.
(53) Vinckier, I.; Laun, H. M. *Macromol. Symp.* **2000**, *149*, 151–156.
(54) Joshi, M.; Butola, B. S.; Simon, G.; Kukaleva, N. *Macromolecules* **2006**, *39*, 1839–1849.
(55) Hohenberg, P. C.; Halperin, B. I. *Rev. Mod. Phys.* **1976**, *49*, 435–479.
(56) Cabral, J. T.; Higgins, J. S.; Yerina, N. A.; Magonov, S. N. *Macromolecules* **2002**, *35*, 1941–1950.
(57) Jupp, L.; Yuan, X. F. *J. Non-Newtonian Fluid Mech.* **2004**, *124*, 93–101.
(58) Lee, H. N.; Riggleman, R. A.; de Pablo, J. J.; Ediger, M. D. *Macromolecules* **2009**, *42*, 4328–4336.
(59) Tsenoglou, C. *Macromolecules* **1991**, *24*, 1762–1767.
(60) Milner, S. T. *J. Rheol.* **1996**, *40*, 303–315.
(61) Lee, H. S.; Kim, E. S. *Macromolecules* **2005**, *38*, 1196–1200.
(62) Kumar, S. K.; Colby, R. H.; Anastasiadis, S. H.; Fates, G. M. *J. Chem. Phys.* **1996**, *105*, 3777–3788.
(63) Lodge, T. P.; McLeish, T. C. B. *Macromolecules* **2000**, *33*, 5278.
(64) Leroy, E.; Algria, A.; Colmenero, J. *Macromolecules* **2002**, *35*, 5587–5590.
(65) Chaffey, C. E.; Brenner, H. *J. Colloid Interface Sci.* **1967**, *24*, 258–269.
(66) Vermant, J.; Van Puyvelde, P.; Moldenaers, P.; Mewis, J.; Fuller, G. G. *Langmuir* **1998**, *14*, 1612–1617.
(67) Lacroix, C.; Aressy, M.; Carreau, P. *Rheol. Acta* **1997**, *36*, 416–428.
(68) Larson, R. G. *The Structure and Rheology of Complex Fluids*; Oxford University Press: New York, 1999.